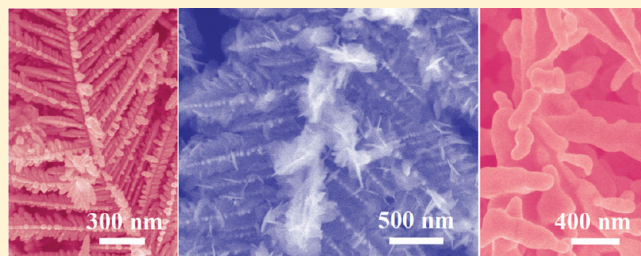# Morphology-Controlled Green Synthesis of Single Crystalline Silver Dendrites, Dendritic Flowers, and Rods, and Their Growth Mechanism

Gaixia Zhang,[†] Shuhui Sun,[†] Mohammad Norouzi Banis,[†] Ruying Li,[†] Mei Cai,[‡] and Xueliang Sun*,[†]

[†]Department of Mechanical and Materials Engineering, The University of Western Ontario, London, Ontario N6A 5B9, Canada

[‡]General Motors Research and Development Center, Warren, Michigan 48090-9055, United States

**ABSTRACT:** Various single-crystalline Ag nanostructures including dendrites, dendritic flowers, and cactus-like rods have been successfully synthesized in high yield through a simple, facile, cost-effective method based on the galvanic replacement reaction. The products were characterized by X-ray powder diffraction (XRD), scanning electron microscopy (SEM), transmission electron microscopy (TEM), high-resolution TEM (HRTEM), and energy dispersive X-ray spectroscopy (EDX). The morphology and structure of Ag products can be well controlled by tuning the concentrations of Ag metal salt precursor. Through a series of time-dependent morphological evolution studies, the growth processes of Ag nanostructures have been systematically investigated and the corresponding growth mechanisms have been discussed.

## 1. INTRODUCTION

The nanostructures of noble metals, especially the relatively low-cost and highly conductive silver, have attracted considerable interest in recent years due to their unique electrical, optical, and thermal properties, as well as their potential applications in (opto)electronic devices,[1] catalysis,[2] and surface-enhanced Raman scattering (SERS) detection.[3,4] The intrinsic properties of the metal nanostructures can be tuned by controlling their shape, size, and crystallinity. To date, many approaches have been developed to prepare Ag nanostructures in different shapes, such as wires,[5−8] belts,[9] rice,[10] ribbons,[11] prisms,[12] sheets,[13,14] cubes,[15] and so on.[16−20] Recently, extensive interest has been expressed in the synthesis of more complex structures that are ideally composed of nanocrystals (particles, rods, ribbons, sheets, and so forth) arranged in a particular way as well as their growth mechanism,[21−25] because such hierarchical materials not only possess improved properties originating from their building blocks but also solve the problem of nanomaterial agglomeration and find applications in many fields. Most hierarchical complex Ag structures reported so far have mainly focused on simple dendrites that consist of several generations of branches with self-similarity.[26−37] The synthetic methods used for such materials include electrochemical deposition,[6,26,27] surfactant process,[28] γ- or ultrasonic irradiation,[29,30] hydrothermal method,[31] template approach,[32] etc. Recently, the formation of silver dendrites via galvanic deposition has been reported using bulk materials (e.g., silicon, aluminum, copper, zinc) as substrates.[31,33−36] In general, the above methods normally involve the reduction of silver salts in the presence of potentiostat or organic surfactants, or at elevated temperature, or requiring the removal of template/substrate to get pure products; moreover, the as-synthesized Ag products are confined in simple dendritic structures. Therefore, it still remains very interesting and challenging to synthesize Ag dendrites with even more complex but adjustable structures through surfactant-free, simpler routes under mild conditions. In addition, a full mechanistic understanding of how or why such structures form still remains challenging.

Here, based on the replacement reaction, we report a simple, cost-effective, and versatile strategy for the large scale synthesis of adjustable 3D Ag nanostructures, such as simple dendrites that have a fractal structure consisting of several generations of branches with lengths up to a few micrometers, dendritic flowers that have a dendritic frame decorated with many self-assembled flower petals, and dendritic rods that have a cactus shaped structure composed of a few generations of rods. In these syntheses, only commercial Mg powder was used as sacrificial metal to react with $AgNO_3$ in aqueous solution, and no organic solvents or capping agents were necessary. The precursor concentration effect of $AgNO_3$ in the morphological control of Ag structures is discussed in detail. Through a series of time-dependent morphological evolution studies, the growth processes of Ag nanostructures have been systematically investigated, and the corresponding growth mechanisms are discussed.

## 2. EXPERIMENTAL SECTION

**Synthesis.** Doubly distilled deionized (DI) water was used for all preparations. Silver nitrate ($AgNO_3$) was obtained from Sigma-Aldrich and used as received. The magnesium metal powder (Mg, $-100 + 200$ mesh, 99.6%) was obtained from Alfa Aesar. In a typical synthesis, a
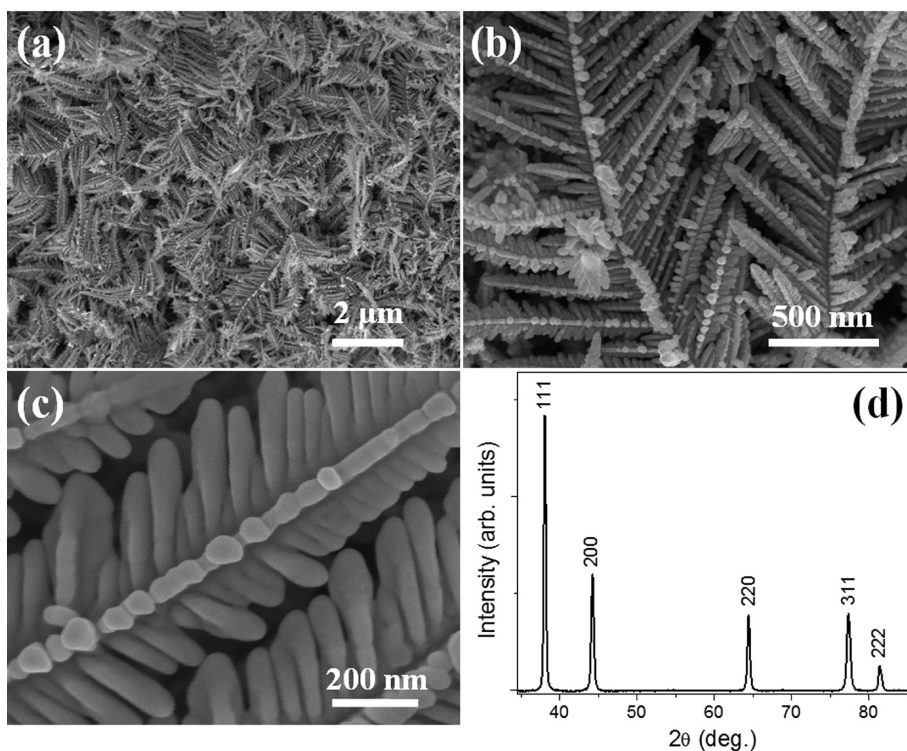
**Figure 1.** (a−c) SEM images at different magnifications and (d) powder XRD patterns of as-synthesized Ag dendrites.

controlled amount of freshly prepared AgNO₃ aqueous solution was quickly added to a glass vial that contained a predetermined amount of commercially available Mg powder. To synthesize simple Ag dendrites, for example, the replacement reaction between Mg (5.3 mg) and AgNO₃ solution (0.03 M, 17 mL) was used, where the atomic concentration of Ag⁺ was over two times greater than that of Mg, so that the Mg would be completely oxidized to Mg²⁺, precipitating Ag dendrites only. For the synthesis of other Ag structures, dendritic flowers, and cactus-like rods, the AgNO₃ concentration was decrease to 0.012 M and increased to 0.1 M, respectively. The reactions were conducted in glass vials (20 mL) at 6 °C in ambient atmosphere for up to several minutes. The temperature was controlled with a constant temperature bath (VWR model 1162A). After the reduction reactions were complete, the products were washed several times in DI water, collected by filtration, and then dried in a vacuum oven overnight.

**Characterization.** The morphologies, crystallinities, and chemical compositions of the samples were determined with a field-emission scanning electron microscope (FESEM, Hitachi S-4800, operating at 5 kV), equipped with an energy-dispersive X-ray spectrometer (EDX), a transmission electron microscope (TEM, Philips CM10, operating at an accelerating voltage of 100 kV), and a high-resolution TEM (HRTEM, JEOL 2010F, operating at 200 kV). Powder X-ray diffraction (XRD) measurements were performed on a Bruker D8 Discover diffractormeter operating at 40 kV and 40 mA, with Cu Kα radiation ($\lambda$ = 0.154 nm). For the time-dependent morphology evolution study, samples, taken from different reaction stages, were washed and placed on silicon wafer substrates, and then dried under ambient conditions.

## 3. RESULTS AND DISCUSSION

Figure 1 shows a typical Ag dendrite structure synthesized by Mg powder and AgNO₃ (0.03 M) in aqueous solution. The low-magnification SEM image (Figure 1a) shows a large quantity of such structure, demonstrating very good uniformity. The higher

magnification SEM images (Figure 1b,c) clearly show the dendrite structures with multilevel generations, having a long main trunk with short side branches (or even further sub-branches), all decorated by small leaves.[21] Generally, the lengths of the trunks and (sub)branches are several tens of micrometers and several micrometers, respectively. However, all the diameters (trunk, branch, and sub-branches) have a similar size of about 40 nm. The XRD pattern of the Ag dendrite (Figure 1d) matches well with the Ag face-centered cubic (fcc) structure (JCPDS, No. 04-0783), indicating its high crystallinity. Further, no other diffraction peaks are observed, indicating its high purity.

A TEM investigation was carried out in order to study the crystal structure of the Ag dendrite. Figure 2a,b show a typical individual branch of Ag dendritic structure at several magnifications. The results are consistent with those observed under SEM investigation. The inset in Figure 2a shows a HRTEM image taken from the root of the trunk (labeled with the square in Figure 2a). The obvious fringes with a ∼0.23 nm interplanar separation correspond to the {111} planes, which indicates that the growth direction of the trunk is along ⟨111⟩. Figure 2c shows a typical HRTEM image recorded from the stem and the junctions of a dendritic branch (indicated by the square in Figure 2b). Interestingly, its growth direction is also along ⟨111⟩. This implies that the Ag dendrites grow along a preferential direction. In addition, this HRTEM image also shows that, because the stem and the side branch have identical crystal orientations, the total dendrite structure is a single crystal. This is further confirmed by the three sets of SAED patterns (taken at different places) with identical diffraction patterns. The same phenomenon (a single crystal with the same lattice orientation) occurs in the structures of branches and leaves, as shown in Figure 2d, where the image was taken at the labeled circle in Figure 2b. This novel, complex, single crystal Ag structure with
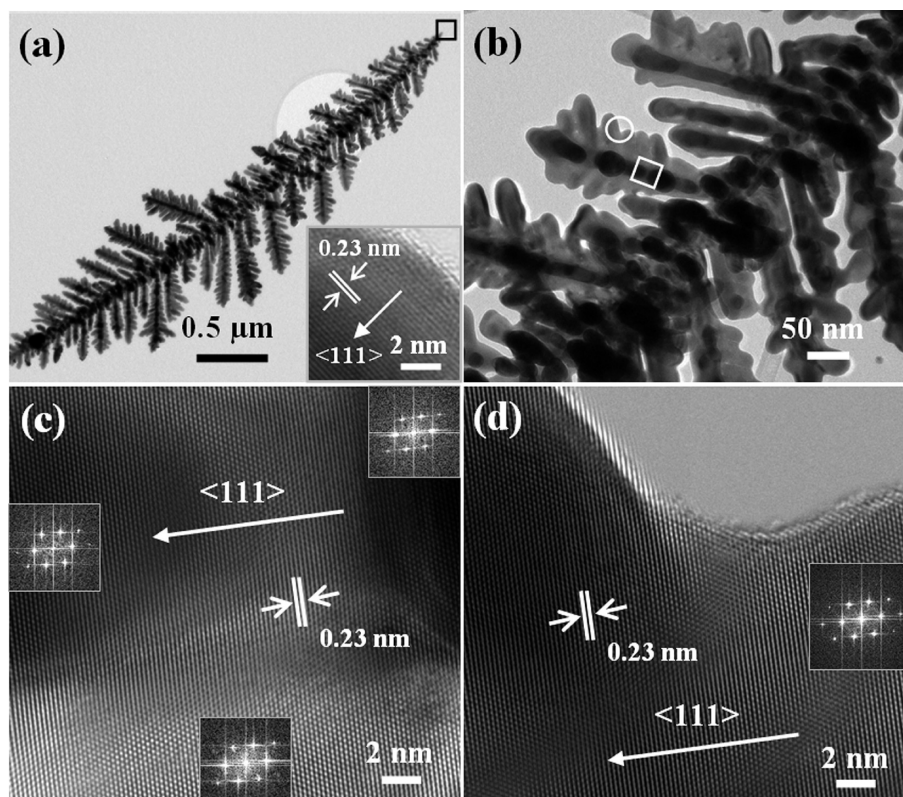
**Figure 2.** (a,b) TEM images and (c,d) HRTEM images of the single crystalline Ag dendrite structures. The insets in parts c and d are the corresponding FFT patterns taken from where they are in the images.

high surface area should have great potential in many applications, such as fuel cells,[38,39] and SERS detection.[3,4]

A morphological evolution study was conducted to obtain a complete view of the Ag dendrite formation process and its growth mechanism. Products were collected at 0.5, 1, 2, 3, 4, and 6 min of reaction time, and their morphologies were evaluated by SEM (Figure 3). When collected after 0.5 min of reaction, the Mg particle surfaces become rough (Figure 3a), decorated with many tiny nanoparticles and various ridgelike structures. After 1 min, those tiny nanoparticles and ridgelike structures grow larger, resulting in very porous Ag structures on the Mg particle surfaces (Figure 3b). Obviously, the growth rate of the former is faster than that of the latter, and most of the time, the nanoparticles self-assemble along the ridgelike structures (indicated by the arrows in Figure 3b). After 2 min, as shown in Figure 3c, the Ag nanoparticles grow/aggregate/self-assemble into rods, further forming rudimentary dendrite structures. After 3 and 4 min, multigeneration Ag dendritic structures are formed, and the Ag branches generated along the ridgelike structures are still obvious (indicated by arrows in Figure 3d,e). After 6 min, larger and smoother Ag dendrite structures, with higher order generations, are finally formed (Figure 3f).

Based on these results, a growth mechanism for the formation of Ag dendrite structures is proposed. A schematic illustration for the evaluation of Ag dendrite structures, together with the corresponding SEM images, is presented in Figure 4. First, the initial replacement reaction between Mg and $Ag^+$ proceeds rapidly, due to the very large difference in their redox potentials, $Mg^{2+}/Mg$ ($-2.356$ V) and $Ag^+/Ag$ (0.799 V) vs the standard hydrogen electrode (SHE).[40] This promotes the random formation of Ag nuclei and ridgelike structures on the Mg particle surfaces (Figure 4b); the reaction appears to preferentially start at the small particles and sharp edges (those areas are relatively more active to react with the solution) of the Mg microparticle surface (indicated, respectively, by dashed and solid arrows in Figure 4a), which are energetically favorable sites.[41−43] In the second stage, the as-formed structures act as the sites for further Ag precipitation. Note that (1) the nanoparticles grow much faster than the ridgelike structures, which is due to the unique high surface energy of the former;[44] and (2) the rapidly precipitated Ag atoms along the ridgelike structures have insufficient time to reorganize and merge into the matrix of ridgelike structures and, thus, act as the sites for further Ag precipitation. This gives the impression of self-assembled nanoparticles along the ridgelike structures. Meanwhile, via coalescence and Ostwald ripening,[45,46] nanoparticles grow and coalesce to form rodlike structures, giving the appearance of forming initial Ag dendrite structures (Figure 4c). In the third stage, on sacrificing Mg atoms, multigenerated Ag dendrite structures are formed (Figure 4d). Further, with Ag atom reorganization, the protruding Ag particles and ridgelike structures merge into the dendritic matrix, finally resulting in perfect Ag dendritic structures with self-similarity (Figure 4d). This is consistent with the previous reported mechanism of nanoparticle-aggregated self-assembly crystallization, talking about a transition from polycrystalline aggregates to a single crystal during the structure growth.[47−49] In addition, Ostwald ripening also plays an important role in forming a smooth surface and regular shape of the final crystal.[50]

In addition, the morphology of the Ag structures can be easily controlled via tuning the $AgNO_3$ solution concentrations.
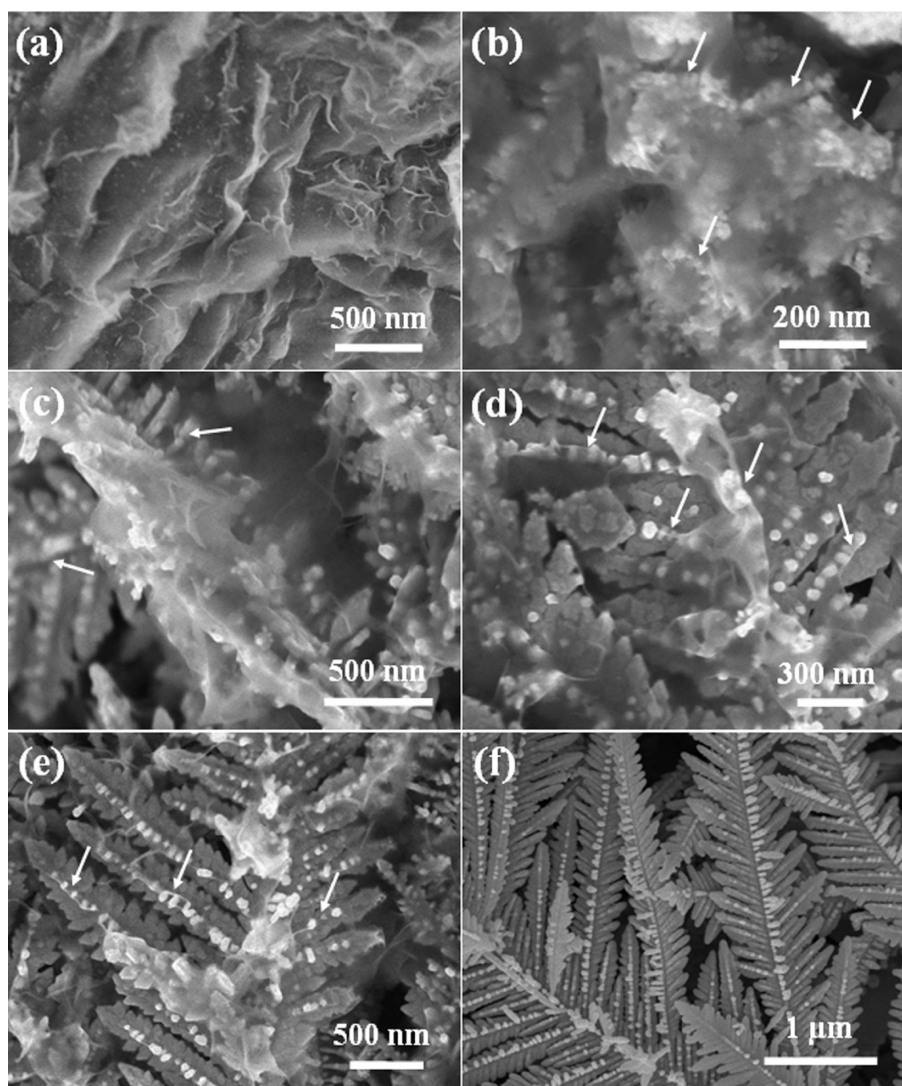
**Figure 3.** SEM investigation of the morphological evolution of Ag dendrites, as a function of Mg particle immersion time in AgNO$_3$ solution for (a) 0.5, (b) 1, (c) 2, (d) 3, (e) 4, and (f) 6 min, respectively.
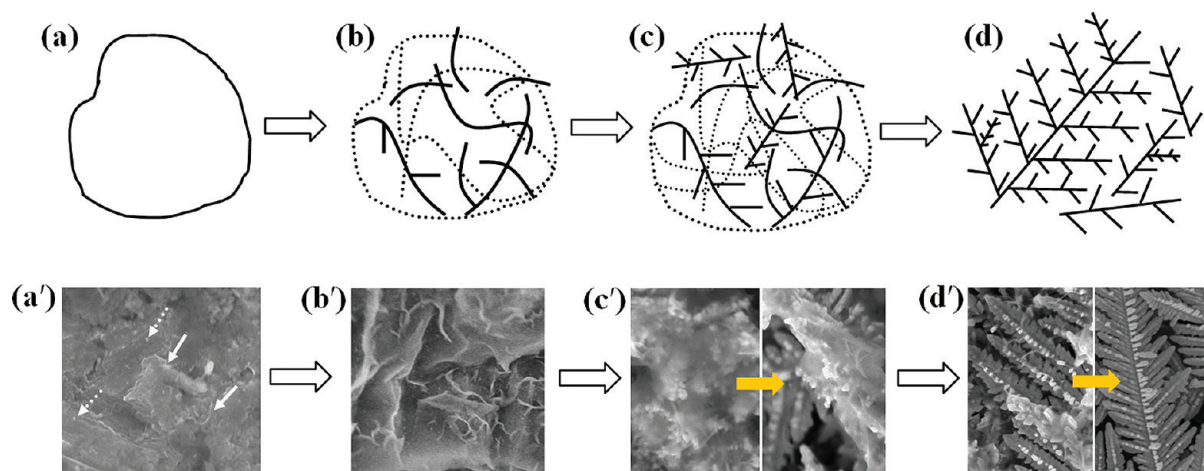


**Figure 4.** Schematic illustration of the formation and morphology evolution of Ag dendrite structures.
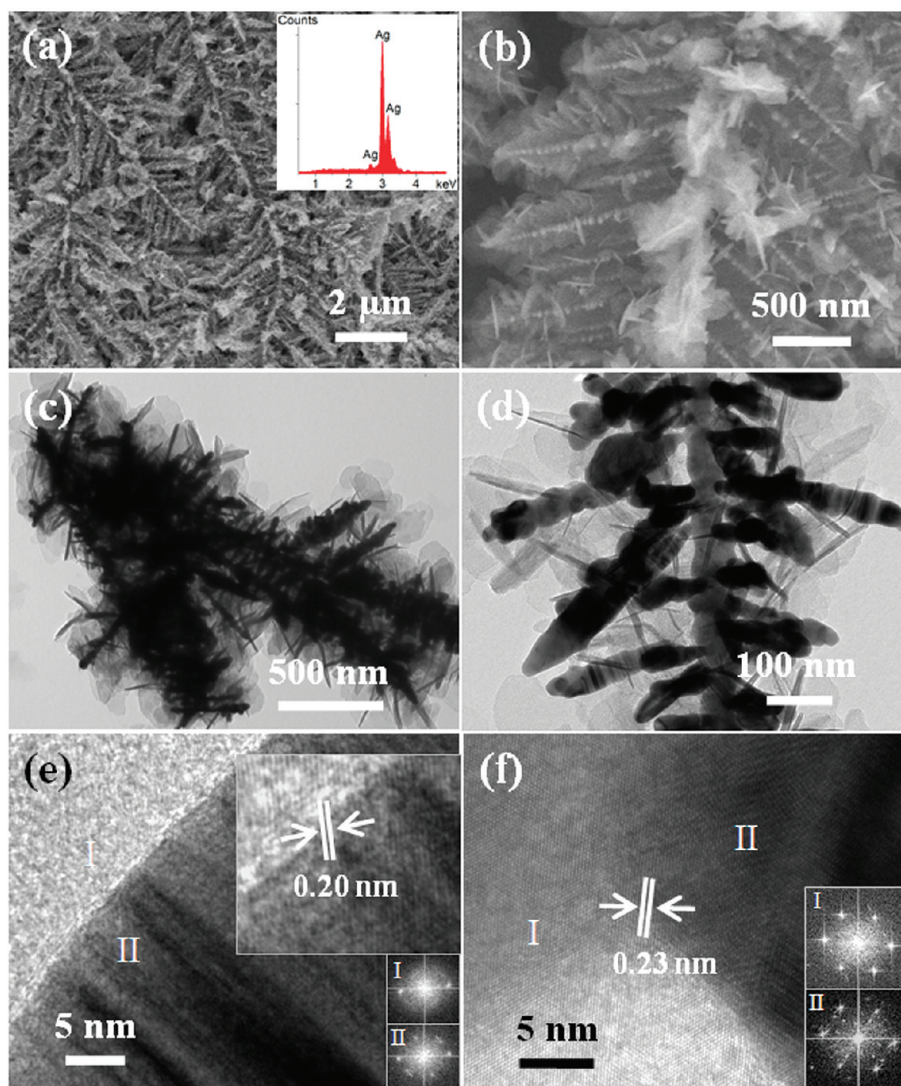
**Figure 5.** Characterization of Ag dendritic flowers obtained by 0.012 M AgNO$_3$: (a, b) SEM images; (c, d) TEM images; (e, f) HRTEM images with corresponding FFT patterns taken from where the uppercase roman numerals indicate.

When 0.012 M AgNO$_3$ was used in the reaction, novel Ag dendritic flowers (a dendritic frame decorated with many self-assembled flower petals), were obtained (Figure 5a,b). To the best of our knowledge, this dendritic flower structure has never been reported before. The EDX spectrum (inset of Figure 5a) demonstrates its high purity. Figure 5c shows a typical TEM image of the Ag dendritic flower composed of a dendritic frame and many thin petals. A higher magnification TEM image with a sparse dendritic frame and flower petals was purposely chosen in order to get HRTEM images (Figure 5d). The two typical HRTEM images (Figure 5e,f) demonstrate that the complex dendritic flower is a single crystal because the dendritic frame and the petals have identical crystal orientations. This is further confirmed by the two sets of FFT patterns taken from the connected dendrite frame and petal, respectively.

When we simply increase the AgNO$_3$ concentration to 0.1 M, dendritic rods, with a cactus structure shape composed of several larger (50–150 nm) rods, were formed (Figure 6). The EDX spectrum (Figure 6c) confirms its purity. The HRTEM image

(Figure 6d) shows its crystallinity. Besides the perfect crystal lattice structures, some obvious defects that mainly contain dislocations and stacking faults[51–53] are also formed, due to the faster reaction rate originating from the higher AgNO$_3$ concentration.

From such experiments, we have found that, with an increase of AgNO$_3$ concentrations from 0.012 to 0.03 to 0.1 M, dendritic flowers, dendrites, and dendritic rods were obtained, respectively. This reinforces our hypothesis proposed for the growth process of the dendrites. That is, with lower AgNO$_3$ precursor concentration, the reaction rate decreases. Therefore, in the case of dendritic flower, the slowly precipitated Ag atoms promote the growth of Ag nuclei (or particles) and ridgelike structures at the same time. Then, via further reorganization of Ag atoms, dendritic flowers are ultimately formed. With higher concentration, the reaction rate increases. Therefore, at the early stages, rapidly precipitated Ag atoms will cover (in the case of Ag dendrites) or ruin (in the case of Ag dendritic rods) the ridgelike structures. Then, with further consumption of Ag$^+$, the reaction rate decreases. Therefore, there is a sufficient time for the reorganization of Ag atoms,
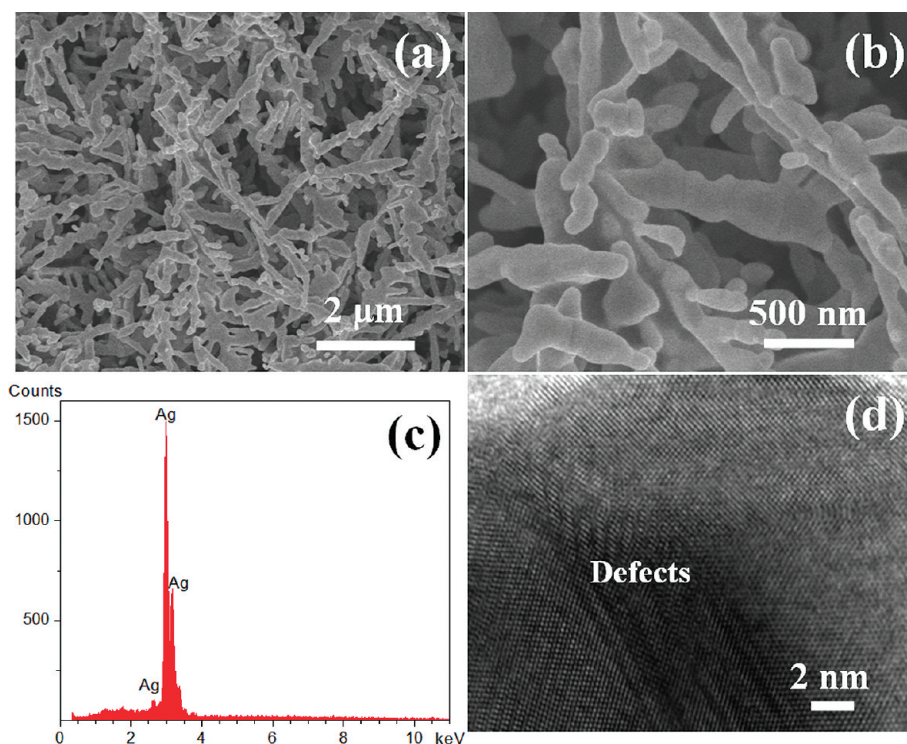
**Figure 6.** Characterization of Ag dendritic rods obtained by 0.1 M AgNO$_3$.

resulting in the final formation of Ag dendrite or dendritic rod structures. Note that, in any case, the previously formed ridgelike structures play a key role that guides the deposition of further precipitated Ag atoms, finally promoting the formation of dendritic structures.

## 4. CONCLUSIONS

In summary, various novel single-crystalline Ag nanostructures, including dendrite, dendritic flower, and rod, have been successfully synthesized on a large scale by a simple, cost-effective, aqueous solution method; the method is based on a galvanic replacement reaction between Mg and AgNO$_3$, without using any template or surfactant. Through a series of time-dependent morphological evolution studies, the growth processes of Ag dendritic structures have been systematically investigated. A precursor concentration effect on the morphological and structural control of the Ag products has also been proposed and discussed. The proposed growth mechanism may guide the study on the formation process of other novel dendritic structures.

## ■ AUTHOR INFORMATION

**Corresponding Author**
*E-mail: xsun@eng.uwo.ca.

## ■ ACKNOWLEDGMENT

## ■ REFERENCES

(1) Wang, H.; Qi, L. *Adv. Funct. Mater.* **2008**, *18*, 1249–1256.
(2) Kostowskyj, M. A.; Kirk, D. W.; Thorpe, S. J. *Int. J. Hydrogen Energy* **2010**, *35*, 5666–5672.
(3) Wiley, B. J.; Chen, Y.; McLellan, J.; Xiong, Y.; Li, Z.-Y.; Ginger, D.; Xia, Y. *Nano Lett.* **2007**, *7*, 1032–1036.
(4) Nie, S.; Emory, S. R. *Science* **1997**, *275*, 1102–1106.
(5) Sun, X.; Li, Y. *Adv. Mater.* **2005**, *17*, 2626–2630.
(6) Fang, J.; Hahn, H.; Krupke, R.; Schramm, F.; Scherer, T.; Ding, B.; Song, X. *Chem. Commun.* **2009**, 1130–1132.
(7) Liu, J.; Tsai, C.; Chiu, Y.; Hsieh, F. *Nanotechnology* **2009**, *20*, No. 035301(10 pp).
(8) Lazzara, T. D.; Bourret, G. R.; Lennox, R. B.; van de Ven, T. G. M. *Chem. Mater.* **2008**, *21*, 2020–2026.
(9) Liu, B.; Zhao, X. *Mater. Res. Bull.* **2009**, *44*, 682–687.
(10) Liang, H.; Yang, H.; Wang, W.; Li, J.; Xu, H. *J. Am. Chem. Soc.* **2009**, *131*, 6068–6069.
(11) Marchal-Roch, C.; Mayer, C. M.; Michel, A.; Dumas, E.; Liu, F. X.; Séchersse, F. *Chem. Commun.* **2007**, 3750–3752.
(12) Zhang, J.; Liu, H.; Zhan, P.; Wang, Z.; Ming, N. *Adv. Funct. Mater.* **2007**, *17*, 1558–1566.
(13) Liu, G.; Ci, W.; Liang, C. *Cryst. Growth Des.* **2008**, *8*, 2748–2752.
(14) Yang, J.; Wang, H.; Zhang, H. *J. Phys. Chem. C* **2008**, *112*, 13065–13069.
(15) Skrabalak, S. E.; Au, L.; Li, X.; Xia, Y. *Nature Protocols* **2007**, *2*, 2182–2190.
(16) Jena, B. K.; Mishra, B. K.; Bohidar, S. *J. Phys. Chem. C* **2009**, *113*, 14753–14758.
(17) Liu, X.; Zhang, F.; Huang, R.; Pan, C.; Zhu, J. *Cryst. Growth Des.* **2008**, *8*, 1916–1923.
(18) Nadagouda, M. N.; Varma, R. S. *J. Nanomaterials* **2008**No. 782358(8 pp).
(19) Zhang, W. C.; Wu, X. L.; Chen, H. T.; Gao, Y. J.; Zhu, J.; Huang, G. S.; Chu, P. K. *Acta Mater.* **2008**, *56*, 2508–2513.
(20) Tsuji, M.; Matsumoto, K.; Jiang, P.; Matsuo, R.; Tang, X.; Kamarudin, K. S. N. *Colloids Surf. A* **2008**, *316*, 266–277.

(21) Liu, X.; Lin, Y.; Zhou, S.; Sheehan, S.; Wang, D. *Energies* **2010**, 3, 285–300.

(22) Ma, X.; Chen, Z. G.; Hartono, S. B.; Jiang, H. B.; Zhou, J.; Qiao, S. Z.; Yang, H. G. *Chem. Commun.* **2010**, 6608–6610.

(23) Chen, J. S.; Chen, C.; Liu, J.; Xu, R.; Qiao, S. Z.; Lou, X. W. *Commun.* **2011**, 2631–2633.

(24) Fang, W Q.; Zhou, J. Z.; Liu, J.; Chen, Z. G.; Yang, C.; Sun, C. H.; Qian, G. R.; Zhou, J.; Qiao, S. Z.; Yang, H. G. *Chem.—Eur. J.* **2011**, 17, 1423–1427.

(25) Yang, H. G.; Sun, C. H.; Qiao, S. Z.; Zhou, J.; Liu, G.; Smith, S. C.; Cheng, H. M.; Lu, G. M. *Nature* **2008**, 453, 638–642.

(26) Zhou, Q.; Wang, S.; Jia, N.; Liu, L.; Yang, J.; Jiang, Z. *Mater. Lett.* **2006**, 60, 3789–3792.

(27) Jing, C.; Fang, Y. *J. Colloid Interface Sci.* **2007**, 314, 46–51.

(28) Fan, L.; Guo, R. *Cryst. Growth Des.* **2008**, 8, 2150–2156.

(29) Wang, S.; Xin, H. *J. Phys. Chem. B* **2000**, 104, 5681–5685.

(30) Wang, X.; Shao, L.; Guo, W.; Wang, J.; Zhu, Y.; Wang, C. *Ultrason. Sonochem.* **2009**, 16, 747–751.

(31) Wang, Z.; Zhao, Z.; Qiu, J. *J. Phys. Chem. Solids* **2008**, 69, 1296–1300.

(32) Xiao, J.; Xie, Y.; Tang, R.; Chen, M.; Tian, X. *Adv. Mater.* **2001**, 13, 1887–1891.

(33) Shi, F.; Song, Y.; Niu, J.; Xia, X.; Wang, Z.; Zhang, X. *Chem. Mater.* **2006**, 18, 1365–1368.

(34) Yang, Y.; Meng, G. *J. Appl. Phys.* **2010**, 107, No. 044315(5 pp).

(35) Gutés, A.; Carraro, C.; Maboudian, R. *J. Am. Chem. Soc.* **2010**, 132, 1476–1477.

(36) He, L.; Lin, M.; Kim, N. *J. Raman Spectrosc.* **2010**, 41, 739–744.

(37) Wang, Y.; Camargo, P. H. C.; Skrabalak, S. E.; Gu, H.; Xia, Y. *Langmuir* **2008**, 24, 12042–12046.

(38) Chen, Z.; Waje, M.; Li, W.; Yan, Y. *Angew. Chem., Int. Ed.* **2007**, 46, 4060–4063.

(39) Bi, Y.; Lu, G. *Chem. Mater.* **2008**, 20, 1224–1226.

(40) Zoski, C. G. *Handbook of Electrochemistry*; Elsevier: Oxford, 2007; pp 815−817.

(41) Sun, S. H.; Meng, G. W.; Wang, Y. W.; Gao, T.; Zhang, M. G.; Tian, Y. T.; Peng, X. S.; Zhang, L. D. *Appl. Phys. A: Mater. Sci. Process.* **2003**, 76, 287–289.

(42) Zhang, G. X.; Sun, S. H.; Zhang, Y.; Li, R. Y.; Cai, M.; Sun, X. L. *Chem. Mater.* **2010**, 22, 4721–4727.

(43) Zhang, G. X.; Sun, S. H.; Ionescu, M. I.; Liu, H.; Zhong, Y.; Li, R. Y.; Sun, X. L. *Langmuir* **2010**, 26, 4346–4350.

(44) Nanda, K. K.; Maisels, A.; Kruis, F. E.; Fissan, H.; Stappert, S. *Phys. Rev. Lett.* **2003**, 91, 106102(4 pp).

(45) Li, C. M.; Robertson, I. M.; Jenkins, M. L.; Hutchison, J. L.; Doole, R. C. *Micron* **2005**, 36, 9–15.

(46) José-Yacamán, M.; Gutierrez-Wing, C.; Miki, M.; Yang, D. Q.; Piyakis, K. N. *J. Phys. Chem. B* **2005**, 109, 9703–9711.

(47) Fang, J.; You, H.; Kong, P.; Yi, Y.; Song, X.; Ding, B. *Cryst. Growth Des.* **2007**, 7, 864–867.

(48) Fang, J.; Ding, B.; Song, X. *Cryst. Growth Des.* **2008**, 8, 3616–3622.

(49) Fang, J.; Ma, X.; Cai, H.; Song, X.; Ding, B. *Nanotechnology* **2006**, 17, 5841–5845.

(50) Fang, J.; Ding, B.; Song, X.; Han, Y. *Appl. Phys. Lett.* **2008**, 92, 173120(3 pp).

(51) Schmitz, S.; Brenker, F. E. *Astrophys. J.* **2008**, 681, L105–L108.

(52) Courty, A.; Henry, A. I.; Goubet, N.; Pileni, M. P. *Nat. Mater.* **2007**, 6, 900–907.

(53) Germain, V.; Li, J.; Ingert, D.; Wang, Z. L.; Pileni, M. P. *J. Phys. Chem. B* **2003**, 107, 8717–8720.